Asociación Argentina
de Mecánica Computacional

Mecánica Computacional Vol XXXVIII, págs. 635-644 (artículo completo)
H.G. Castro, J.L. Mroginski, R.R. Paz, M.A. Storti (Eds.)
Resistencia, 1-5 Noviembre 2021

PERFORMANCE OF SYSTEM IDENTIFICATION METHODS IN STRUCTURAL DYNAMICS

Leandro E. Nardi[a], Oscar Möller[a] and Juan P. Ascheri[a]

[a]*Instituto de Mecánica Aplicada y Estructuras (IMAE), Facultad Cs.Ex., Ingeniería y Agrimensura, Universidad Nacional de Rosario, Riobamba y Berutti, 2000 Rosario, Argentina,*
lnardi@fceia.unr.edu.ar

Keywords: System Identification, dynamic parameters, vibrations, structural health, civil structures.

Abstract. Structural health monitoring aims at early detection of damage in structural systems and represents a convenient strategy to reduce maintenance and repair costs. An important step in this process is to identify dynamic parameters like frequencies, mode shapes and damping ratios, from accelerations recorded at certain points of the structure. The most widely used method for this is the Peak Picking, based on the Fourier transform. Other methods, originally developed for electronic control, are the subspace identification algorithms formulated in state space. In this paper, the performance of these methods was evaluated when they were applied to a steel beam. Different types of dynamic actions were analysed using numerical results, including free vibrations, harmonic loads and triangular pulse loads. Subsequently, experimental measurements were taken on a physical model subjected to free vibrations and forced vibrations produced by a passing vehicle. It is remarkable that the algorithms work with accuracy in some cases if the input remains unknown, but some information might be necessary to make a correct identification in case of specific types of loads.

1 INTRODUCTION

Structural health monitoring is a key aspect for maintenance and conservation of a society infrastructure. Within the usual classification, there are four discriminated levels of damage studying: damage detection, damage location, damage quantification and remaining service life prediction (Peeters, 2000). Based on the fact that a change in rigidity of some part of the structure modifies its dynamic properties, it is possible to design damage detection techniques from experimental vibration measurements (Thöns *et al.*, 2018). The aim is to reconstruct a mathematical model in state space and determine properties of the studied system, which allow calibrating or optimizing parameters of finite element models (FEM) and detecting damage (Rucevskis and Wesolowski, 2010; Frans, Arfiadi and Parung, 2017; Gorgin, 2020).

This paper analyses the performance of systems identification algorithms on a steel beam resting on simple supports and a cantilever. The process is applied with results obtained from a finite element analysis and with experimental measurements, considering in both cases different loads in the structure. Dynamics responses are acquired with a FEM for free vibrations, harmonic loads and triangular pulse loads. System identification algorithms are then applied to these results and properties of the original structure are determined contemplating the case of knowing the load in the structure and the case where it remains unknown. The experimental measurements on the physical model include free vibrations caused by an impulsive load and forced vibrations produced by a moving load, intending to represent the effects of a passing vehicle. After applying the algorithms, dynamic properties of the structure are determined and compared with the ones obtained from the FEM.

2 METHODS

2.1 Structural Dynamics

While real structures are systems with distributed parameters, a very good approximation can be made using the finite element method, reducing the problem to a system of N degrees of freedom. The behaviour of this system is defined by its dynamic equilibrium equations:

$$\mathrm{m}\ddot{\mathrm{v}}(\mathrm{t}) + \mathrm{c}\dot{\mathrm{v}}(\mathrm{t}) + \mathrm{kv}(\mathrm{t}) = \mathrm{p}(\mathrm{t}) \tag{1}$$

Where $\boldsymbol{m} \in \mathbb{R}^{NxN}$, $\boldsymbol{c} \in \mathbb{R}^{NxN}$ y $\boldsymbol{k} \in \mathbb{R}^{NxN}$ are the mass, damping and stiffness matrices, $\boldsymbol{v}(t) \in \mathbb{R}^{N}$ is the displacement vector and $\boldsymbol{p}(t) \in \mathbb{R}^{N}$ is the external load vector.

The traditional solution in structures is to solve the associated undamped system, obtaining a set of real eigenvectors. If proportional damping is not assumed, the modal matrix cannot be normalized to real values (Prells and Friswell, 2000). In the case of complex eigenvalues, and in the case of structures with low damping, both the eigenvalues and the associated eigenvectors occur in conjugate pairs (Tisseur and Meerbergen, 2001).

2.2 State space formulation

The set of N second order differential equations mentioned above can be expressed in state space by 2N first order differential equations:

$$\dot{\mathrm{X}}(\mathrm{t}) = \mathrm{A_c X}(\mathrm{t}) + \mathrm{B_c u}(\mathrm{t}) \tag{2}$$

Where $\boldsymbol{A_c} \in \mathbb{R}^{nxn}$ is the system state matrix, $\boldsymbol{B_c} \in \mathbb{R}^{nxm}$ is the input matrix, $\boldsymbol{X}(t) \in \mathbb{R}^{n}$ is the state vector and $\boldsymbol{u}(t) \in \mathbb{R}^{m}$ is the input vector. In general, the observation of all degrees of freedom is not possible, obtaining only a set of *l* outputs:

$$\mathrm{y}(\mathrm{t}) = \mathrm{C_c X}(\mathrm{t}) + \mathrm{D_c u}(\mathrm{t}) \tag{3}$$

Where $\boldsymbol{C_c} \in \mathbb{R}^{\boldsymbol{lxn}}$ is hte output matrix, $\boldsymbol{D_c} \in \mathbb{R}^{\boldsymbol{lxm}}$ is the direct transmission matrix and $\boldsymbol{y}(t) \in \mathbb{R}^{\boldsymbol{l}}$ is the output vector.

The solution obtained in state space in the complex field numbers can be expanded to obtain a closed solution in the real field (Mendoza Zabala, 1996), and can be expressed as a linear combination of vectors with real components. In the case of a specific pair of conjugate complex eigenvectors, the solution can be expressed in terms of the real vectors shown in equation (5).

$$\widehat{\mathrm{V}}_{\mathrm{j}} = \widehat{\mathrm{V}}_{\mathrm{jR}} + \mathrm{i}\widehat{\mathrm{V}}_{\mathrm{jI}}\,, \quad \overline{\widehat{\mathrm{V}}_{\mathrm{j}}} = \widehat{\mathrm{V}}_{\mathrm{jR}} - \mathrm{i}\widehat{\mathrm{V}}_{\mathrm{jI}} \tag{4}$$

In case of proportional damping, both vectors are linearly dependent (Prells and Friswell, 2000), and only one of them can be taken to represent the mode shape.

2.3 State space formulation in discrete time

In experimental work, data are sampled at certain time interval *T* obtaining measurements in the time instants $t = kT$, with $k = 0, 1, 2, \dots, j-1$. Since both measurements and the system are susceptible to noise, the error must be incorporated into the general model:

$$\mathrm{x_{k+1}} = \mathrm{Ax_k} + \mathrm{Bu_k} + \mathrm{w_k} \tag{5}$$

$$\mathrm{y_k} = \mathrm{Cx_k} + \mathrm{Du_k} + \mathrm{v_k} \tag{6}$$

Where $\boldsymbol{A} \in \mathbb{R}^{\boldsymbol{nxn}}$, $\boldsymbol{B} \in \mathbb{R}^{\boldsymbol{nxm}}$, $\boldsymbol{C} \in \mathbb{R}^{\boldsymbol{lxn}}$ y $\boldsymbol{D} \in \mathbb{R}^{\boldsymbol{lxm}}$ are the system matrices, $\boldsymbol{x_k} \in \mathbb{R}^{\boldsymbol{n}}$ is the state vector, $\boldsymbol{u_k} \in \mathbb{R}^{\boldsymbol{m}}$ is the input vector, $\boldsymbol{y_k} \in \mathbb{R}^{\boldsymbol{l}}$ is the output vector, $\boldsymbol{w_k} \in \mathbb{R}^{\boldsymbol{n}}$ is the noise process vector and $\boldsymbol{v_k} \in \mathbb{R}^{\boldsymbol{l}}$ is the noise output vector, both zero mean.

The relation between the system matrices in continuous time and in discrete time is presented in equation (17) (Juang, Phan, and Dewell, 2002).

$$\mathrm{A} = \mathrm{e}^{\mathrm{A_c T}}\,, \quad \mathrm{B} = \left[\int_0^{\mathrm{T}} \mathrm{e}^{\mathrm{A_c}\tau}\mathrm{d}\tau\right]\mathrm{B_c}\,, \quad \mathrm{C} = \mathrm{C_c}\,, \quad \mathrm{D} = \mathrm{D_c} \tag{7}$$

It is computationally more convenient to perform the transformation between continuous and discrete time using a bilinear or Tustin transform (Al-Saggaf and Franklin, 1988).

2.4 System identification

Given s measurements of the input $\boldsymbol{u_k} \in \mathbb{R}^{\boldsymbol{m}}$ and the output $\boldsymbol{y_k} \in \mathbb{R}^{\boldsymbol{l}}$, the problem of system identification consists of determining:

- The order of the system n
- The system matrices $\boldsymbol{A} \in \mathbb{R}^{\boldsymbol{nxn}}$, $\boldsymbol{B} \in \mathbb{R}^{\boldsymbol{nxm}}$, $\boldsymbol{C} \in \mathbb{R}^{\boldsymbol{lxn}}$ and $\boldsymbol{D} \in \mathbb{R}^{\boldsymbol{lxm}}$
- The covariance matrices $\boldsymbol{Q} \in \mathbb{R}^{\boldsymbol{nxn}}$, $\boldsymbol{S} \in \mathbb{R}^{\boldsymbol{nxl}}$ and $\boldsymbol{R} \in \mathbb{R}^{\boldsymbol{lxl}}$

The subject is widely treated in (Van Overschee and De Moor, 1996). Two of the most important algorithms Numerical Algorithm for Subspace State Space System Identification (N4SID) (Van Overschee and De Moor, 1994) and Multivariable Output Error State Space (MOESP) (Verhaegen, 1994) differ in the way that matrices of the system are obtained, treated in the cited bibliography.

2.5 Determination of system parameters

Taking s_i as a particular eigenvalue of the matrix $\boldsymbol{A_c}$, the undamped frequency, the damping ratio and the damped frequency can be obtained as follows:

$$\omega_{\mathrm{i}} = |\mathrm{s_i}|\,, \quad \xi_{\mathrm{i}} = \frac{-\mathrm{Re}(\mathrm{s_i})}{\omega_{\mathrm{i}}}\,, \quad \omega_{\mathrm{Di}} = \mathrm{Im}(\mathrm{s_i}) \tag{8}$$

If $\widehat{\boldsymbol{V}}_{\boldsymbol{j}}$ is an eigenvector of the matrix $\boldsymbol{A_c}$, the mode shapes $\widehat{\boldsymbol{\Phi}}_{\boldsymbol{j1}}$ and $\widehat{\boldsymbol{\Phi}}_{\boldsymbol{j2}}$ in structural

coordinates are obtained from the vectors $\widehat{\boldsymbol{V}}_{\boldsymbol{jR}}$ and $\widehat{\boldsymbol{V}}_{\boldsymbol{jI}}$ presented in equation (4) as follows:

$$\widehat{\Phi}_{j1} = C_c \cdot \widehat{V}_{jR} \quad , \quad \widehat{\Phi}_{j2} = C_c \cdot \widehat{V}_{jI} \tag{9}$$

3 ANALYSED STRUCTURE

The structure under study is an IPN100 beam of 6.77 m long, with a central span of 5.00 m and a cantilever at both sides, one of 0.10 cm and the other of 1.67 m, placed on two point supports. The mass per unit length of the beam is 8.34 Ns^2/m^2 and the cross sectional moment of inertia about horizontal axis is 12.2 cm^4, corresponding to bending in the analysed plane respect to the minor axis of the IPN100. In order to materialize each pinned support with the least possible resistance to rotation, two hollow cone-shaped cavities are machined on the beam's flanges, one on each side. The beam is then suspended by means of horizontal cone-tip bolts that fit into the flanges cavities and that are fixed to concrete pillars with fragments of a UPN300 rolled section. Figure 1 shows details of the setup. For low-intensity vibrations, the weight of the profile is sufficient to prevent lifting of the supports.

Figure 1: Dynamic test setup

4 NUMERICAL RESULTS

In the first part of the work, a FEM of the structure is made to know its dynamic properties and evaluate the response to three types of loads. The FEM is made with elements rounding 50 cm long, and classical Rayleigh damping is used with ξ = 2% set for the two first modes. An outline of the model geometry can be seen in Figure 2.

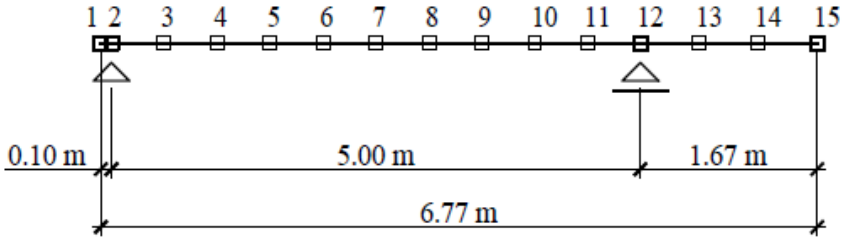

Figure 2: FEM used for structural analysis

The structure is analysed under the application of three different cases of loads. In all situations, the time discretization is performed with T=1 ms. The studied cases are free vibration, where the structure is subjected to a triangle short pulse applied at node 8, harmonic load whit a sinusoidal load applied at node 9, and pulse loads where the structure is subjected to two triangle pulse applied at nodes 6 and 14, with a duration of 1 second. The 2048 acceleration data in nodes 8 and 15 are taken as observed outputs for each type of loads. The algorithm is applied varying the order of the system from n=2 to n=20, with a number of row block of 80, and the frequencies obtained are plotted in the stabilization diagram. The results of natural frequencies are presented in Table 1.

Mode	ω_{FEM} [rad/seg]	$\omega_{Free\ Vibration}$ [rad/seg]	$\omega_{Harmonic}$ [rad/seg]		$\omega_{Pulse\ Loads}$ [rad/seg]	
		Output-Only (N=12)	Output-Only (N=14)	Input-Output (N=14)	Output-Only (N=20)	Input-Output (N=12)
1	18.69	18.69	18.69	18.69	18.73	18.69
2	46.07	46.07	46.07	46.07	45.95	46.08
3	100.91	100.91	100.91	100.91	101.86	100.96
4	205.22	205.22	205.22	205.22	199.98	206.62
5	326.60	326.63	326.63	326.63	331.19	324.66
6	399.80	400.39	403.75	404.04	-	-

Table 1: Natural frequencies obtained from FEM and from system identification algorithms.

The frequencies identified in free vibration are almost the same obtained in the FEM up to the sixth mode. With the harmonic load, both output-only and input-output algorithms show similar results, regardless of the information of the load applied. The output-only method works properly because the sine load can be described in the state space representation, and the algorithm identifies the load frequency too, allowing then to subtract it from the set. For the pulse loads, the frequencies match quite well in the case of input-output, but there are greater differences in the output-only analysis. Conclusion regarding damping ratios obtained from system identification (not included here) are similar to frequencies. In free vibration and harmonic load, the values match those of the FEM, while for charge pulses the difference is greater in the case where the load is not incorporated as data.

In order to obtain mode shapes, accelerations at nodes 4, 6, 8, 10, 13 and 15 are now entered as observed outputs for harmonic and pulse loads. The results are presented in in Figure 3 for the most interesting case where the input is unknown.

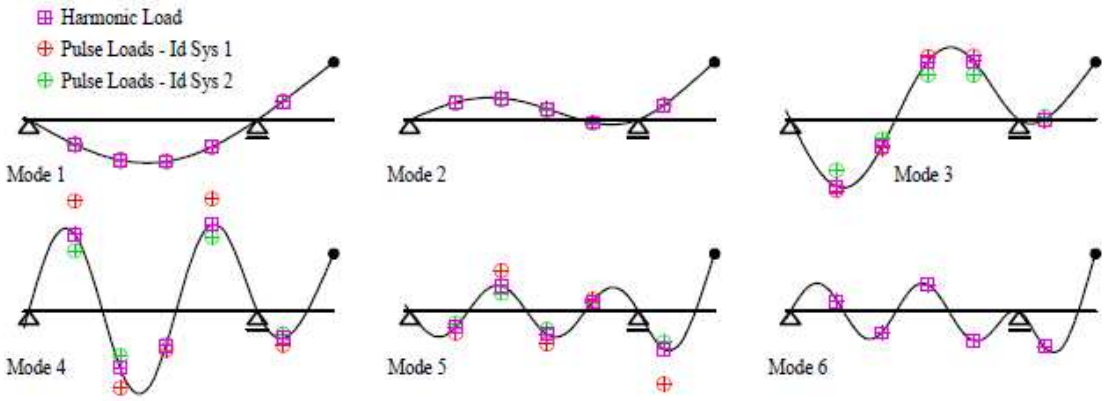

Figure 3: Mode shapes obtained from system identification algorithm where non-zero input remains unknown.

Working with a numerical model and not having perceptible error, the amplitude of the mode shapes would match almost perfectly in all cases where input is provided. When the load remains unknown, in harmonic load case modes obtained match the original shapes, and only one mode is obtained for each natural frequency, according to proportional damping. For pulse loads, differences are larger and two different modes for each natural frequency are obtain with the pulse loads, showing non-proportional damping where it was set proportional.

5 EXPERIMENTAL RESULTS

The aim of the second part of this work is to determine natural frequencies and mode shapes in the real structure, presented in Figure 1. Only two accelerometers are used for the test, so sequential measurements are made with a fixed reference accelerometer left at the end of the cantilever (coordinate $x = 6{,}67\ m$), while the other accelerometer is placed at different points of the beam, changing through coordinates $x = 1{,}00\ m$, $x = 2{,}00\ m$, $x = 2{,}50\ m$, $x = 3{,}00\ m$, $x = 4{,}00\ m$, and $x = 5{,}83\ m$, in which the modal component of the vector at each of the six points is determined. The component at the reference coordinate ($x = 6{,}67\ m$) is set as 1, so that the other coordinates will have a magnitude relative to it.

A new FEM beam with plate elements of 1 cm x 1 cm size is made for this stage, giving more accurate results to compare with the real structure.

5.1 Load cases

The structure is analysed under the application of two different cases of loads. In all measurement sets, the sampling period is T=0.4883 ms (sampling frequency of 2048 Hz), and 8192 acceleration data are analysed.

- Free vibration: The excitation in the structure in the six measurements is achieved with a small stroke at the coordinate $x = 3{,}00\ m$. The response is studied after the impact, obtaining a free vibration in the structure. As an example, data obtained from one measurement set and the Fourier transform are presented in Figure 4.

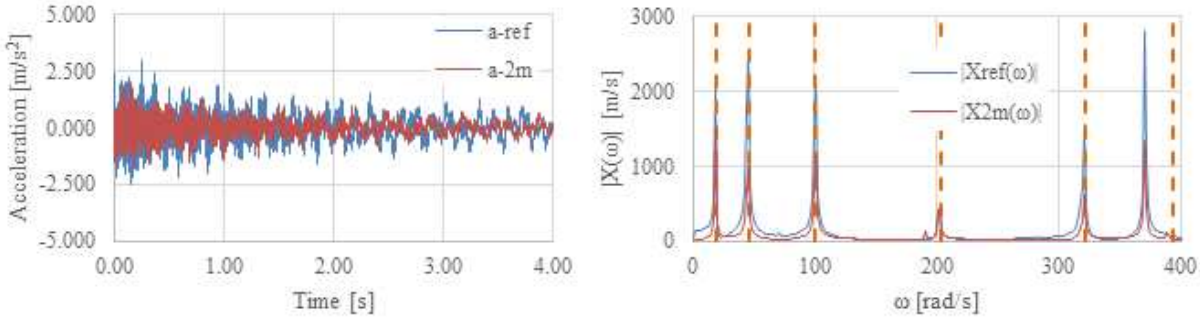

Figure 4: Left: Acceleration response at coordinates x=6.67m and x=2.00m for the free vibration case. Right: Fourier spectrum of the response. Orange lines correspond to FEM natural frequencies.

- Moving Load: In order to simulate vehicles in bridge structures, the metal profile was subjected to the passage of a ball, consisting of an expanded polystyrene hollow sphere filled with concrete, having a total weight of 11.97 N and 12.7 cm diameter. It fits into the metal profile flanges, rolling at an approximate speed of 1.5 m/s. An example of data obtained from one measurement set and the Fourier transform are presented in Figure 5.

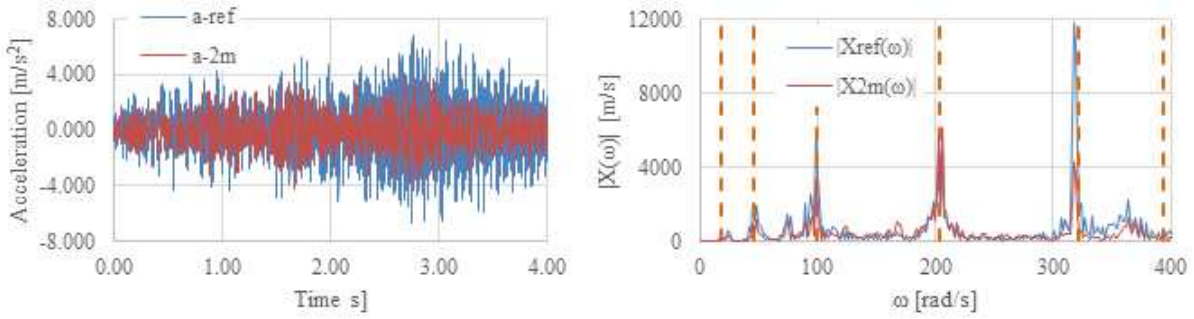

Figure 5: Left: Acceleration response at coordinates x=6.67m and x=2.00m for the moving load case. Right: Fourier spectrum of the response. Orange lines correspond to FEM natural frequencies.

5.2 Identification process

The 8192 acceleration data for every measurement set are taken as observed outputs for each type of loads. An output-only system identification algorithm is made in both cases, where a row block number of 200 is used. The algorithm is applied varying the order of the system from n=2 to n=40, and the frequencies obtained are plotted in the stabilization diagrams. As an illustration, processed results of the measurements presented before at coordinates x=6.67 and x=2.00 are shown in Figure 6.

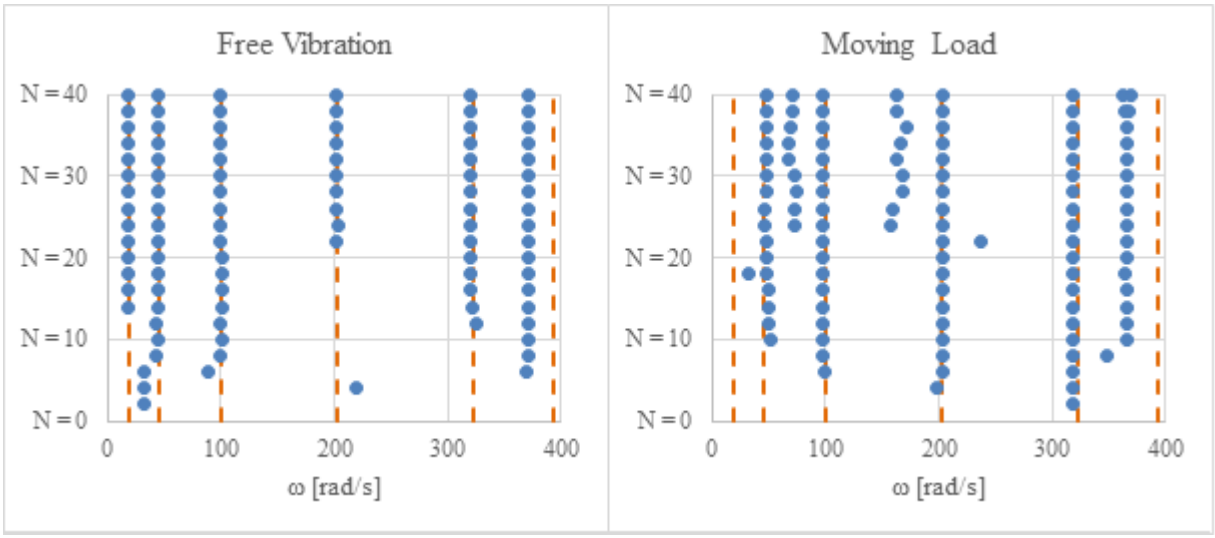

Figure 6: Stabilization diagram for free vibration and moving load in output-only analysis. Orange lines correspond to FEM natural frequencies.

As can be seen in the free vibration case, for low system order, spurious modes that do not correspond to structure frequencies appear. From system orders of approximately 22, the points are stabilized around the reference lines, and spurious values only appear at high frequencies (not shown in the graphic scale). For the passing mass, the results stabilize around the reference lines, but there are more spurious points between them, that seems to stabilize around some value that do not correspond to a natural frequency of the structure. This might be caused by the fact the load is unknown, becoming a difficulty to the process.

The frequencies identified in the case of free vibration are almost the same obtained in the FEM up to the fifth mode, and the sixth frequency shows a difference of 5%. For the moving load, the frequencies match quite well but show a slight greater difference comparing to the free vibration. The first mode did not appear in the identification results, probably because of

the very low participation for the load, which can be seen in the spectrum shown in Figure 5.

The results of natural frequencies and damping ratios are presented in Table 2, corresponding to the order of the system that best matches the natural frequencies of the model.

Mode	ω_{FEM} [rad/seg]	$\omega_{Free\ Vibration}$ [rad/seg]	$\omega_{Moving\ Load}$ [rad/seg]	ξ_{FEM}	$\xi_{Free\ Vibration}$	$\xi_{Moving\ Load}$
		Output-Only (N=40)	Output-Only (N=40)		Output-Only (N=40)	Output-Only (N=40)
1	18.50	18.79	-	0.0200	0.0018	-
2	45.58	45.09	46.67	0.0200	0.0009	0.0259
3	99.80	99.88	98.03	0.0338	0.0006	0.0250
4	202.79	201.84	203.94	0.0646	0.0005	0.0092
5	322.22	316.33	318.23	0.1014	0.0018	0.0081
6	393.59	372.19	363.88	0.1235	0.0008	0.0103

Table 2: Natural frequencies and damping ratios obtained from FEM and from system identification algorithms.

Free vibration throws much lower damping ratios than 2% usually taken in metal structures. This can be explained because of the simplicity of the structure and the lack of joints and other elements that produce a major damp. In the case of moving load, the difference with the model appears too, although the obtained values differ from the ones found in the free vibration case. As it is known, the damping ratio is more difficult to identify than eigenfrequencies.

In order to make a qualitative evaluation of the identified system, some of the outputs are reconstructed using the system state space equations obtained and compared to the original outputs, and plotted in Figure 7. To make a correct visualization, only 0.5 seconds of the records are shown.

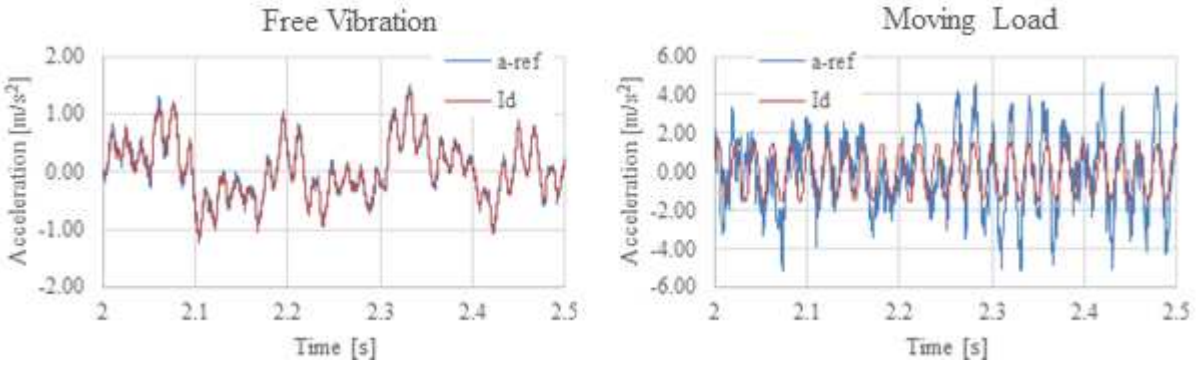

Figure 7: Comparison between original outputs in reference coordinate and obtained with the system state space equations identified in output-only analysis with N=40.

The reconstruction of the outputs matches the original data in the case of free vibration. However, in the case of the moving load, the identification estimated outputs differ from the original record. Figure 7 shows that despite not matching the response, the frequency still remains similar. This last observation may not be the same in the general case, and care should be taken to avoid making a mistake in the identification process.

5.3 Mode shapes

With the six sequential measurements made for both load cases, the mode shapes are obtained. The component at the reference coordinate ($x = 6{,}67\ m$) is set as 1, so that the other coordinates will have a magnitude relative to it. The first six mode shapes obtained for $N = 40$

are shown in the Figures 8 and 9. In state space representation, two conjugate complex eigenvalues for natural frequency are obtained, and two conjugated complex eigenvectors associated to them. The difference between the two modes obtained for each frequency by the system identification method does not necessarily suggest the presence of non-proportional damping, as there may exist other causes that explain these differences.

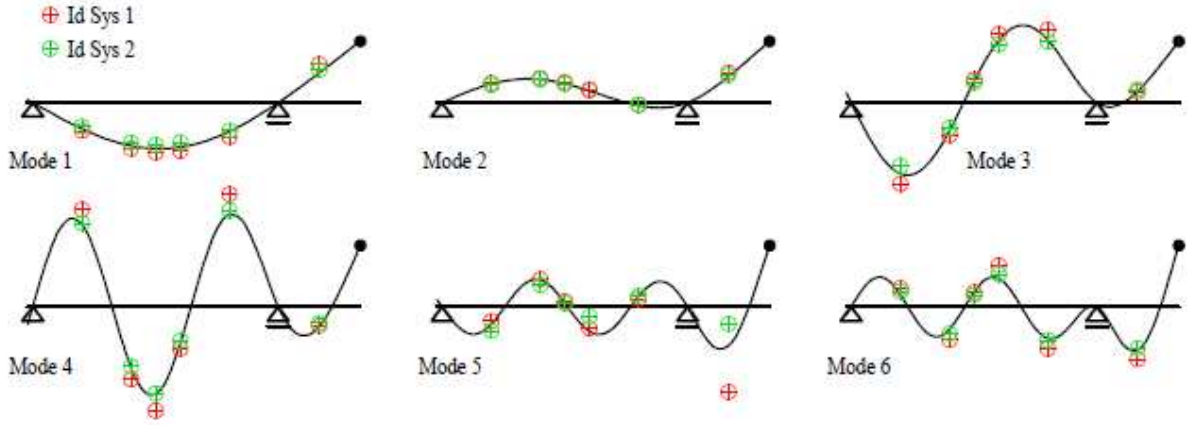

Figure 8: Mode shapes obtained from system identification algorithm for free vibration. The two modes obtained for each frequency are plotted in red and green dots.

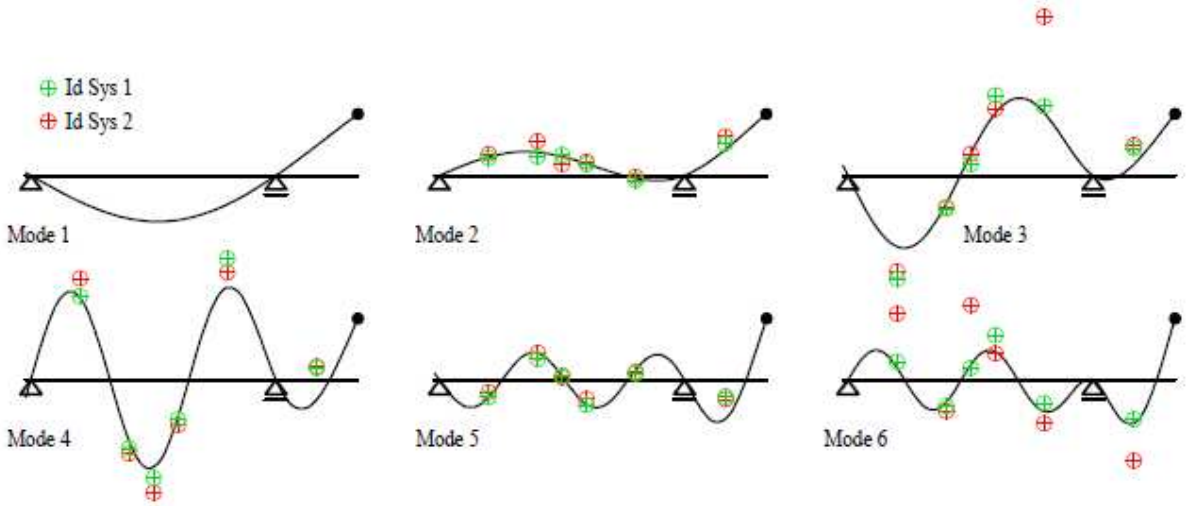

Figure 9: Mode shapes obtained from system identification algorithm for moving load. The two modes obtained for each frequency are plotted in red and green dots. First mode was not detected.

It is observed that the mode shapes found in the coordinates under study make a good match in the case of free vibration, especially up to the third one, presenting greater significant variations for the fourth and higher modes. The modes obtained with the passing mass have greater mismatches, and the first one cannot be detected.

6 CONCLUSIONS

System identification algorithms were applied to numerical and experimental results, obtaining natural frequencies, damping ratios, mode shapes and reconstruction of the original signal. Process applied to finite element results showed that modal parameters can be identified with no error in case of free vibration and harmonic load, and require the knowledge of the input for pulse loads. This fact may be extrapolated to a more general load, especially traffic

load, case of importance in the analysis of a bridge. Experimental results concur with the above conclusion, since frequencies and mode shapes were obtained with a great accuracy for free vibration, but presented bigger differences with the moving load through the structure. In this situation, the error in frequencies is not that big, but mode shapes show a remarkable mismatch. Signal reconstruction enforces this idea, since the identified state space models with unknown inputs were not able to make a good match. Differences presented in output-only identification algorithms suggest that better identification can be made in case of free vibration or harmonic excitation, and have some error in a more general load case. These differences may not affect the frequency estimation, but can represent an important uncertainty if working with mode shapes is desired.

REFERENCES

Al-Saggaf, U. M., & Franklin, G. F, Model Reduction Via Balanced Realizations: An Extension and Frequency Weighting Techniques. *IEEE Transactions on Automatic Control*, 33(7):687-692, 1988.

Frans, R., Arfiadi, Y., & Parung, H, Comparative study of mode shapes curvature and damage locating vector methods for damage detection of structures. *Procedia Engineering*, 171:1263-1271, 2017.

Gorgin, R., Damage identification technique based on mode shape analysis of beam structures. *Structures,* 27:2300–2308, 2020.

Juang, J-N., Phan, M. Q., & Dewell, L., Identification and Control of Mechanical Systems. *Cambridge: Cambridge University Press*, 2001.

Mendoza Zabala, J. L., State-space formulation for structure dynamics [Master Thesis]. *Massachusetts: Massachusetts Institute of Technology*, 1996.

Peeters, B., System identification and damage detection in civil engineering [PhD thesis]. *Leuven: K.U.Leuven.* 2000.

Prells, U., & Friswell, M. I., Measure of non-proportional damping. *Mechanical Systems and Signal Processing*, 14(2):125-137, 2000.

Rucevskis, S., & Wesolowski, M., Identification of damage in a beam structure by using mode shape curvature squares. *Shock and Vibration,* 17:601–610, 2010.

Thöns, S., Döhler, M., Long, L., & Thöns, S., On Damage Detection System Information for Structural Systems. *Structural Engineering International.* 28(3):255-268, 2018.

Tisseur, F., & Meerbergen, K., The quadratic eigenvalue problem. *SIAM Review*, 43(2):235-286, 2001.

Van Overschee, P., & De Moor, B., N4SID: Subspace algorithms for the identification of combined deterministic-stochastic systems. *Automatica,* 30(1):75-93, 1994.

Van Overschee, P., & De Moor, B., Subspace Identification for Linear Systems: Theory - Implementation - Applications. *Leuven: Kluwer Academic Publishers*, 1996.

Verhaegen, M. (1994). Identification of the deterministic part of MIMO state space models given in innovations form from input-output data. *Automatica,* 30(1):61-74, 1994.